

THE EXTENDED MID-INFRARED STRUCTURE OF THE CIRCINUS GALAXY

CHRISTOPHER PACKHAM,¹ JAMES T. RADOMSKI,¹ PATRICK F. ROCHE,² DAVID K. AITKEN,³ ERIC PERLMAN,⁴
ALMUDENA ALONSO-HERRERO,⁵ LUIS COLINA,⁵ AND CHARLES M. TELESCO¹

Received 2004 July 20; accepted 2004 November 23; published 2004 December 6

ABSTRACT

We present subarcsecond resolution mid-IR images of the Circinus galaxy at 8.74 and 18.33 μm . We resolve extended emission at both wavelengths, extending $\sim 2''$ from each side of the nucleus in an approximate east-west direction. These extensions are spatially coincident with previously detected compact (~ 30 pc) V-shaped [O III] emission extending northwest of the nucleus as well as countercone [Si VI] emission, emission at these wavelengths interpreted as delineating the interface between inflowing material and the ionization cone. We detect no extended mid-IR emission associated with the structure responsible for collimating the ionizing photons (i.e., obscuring torus or disk of material), limiting the flux density of the obscuring structure to ≤ 0.27 mJy or a diameter of $\leq 0''.20$ (≤ 4 pc).

Subject headings: galaxies: active — galaxies: individual (Circinus) — galaxies: nuclei — galaxies: Seyfert — infrared: galaxies

1. INTRODUCTION

The Circinus galaxy (hereafter Circinus), at a distance of ~ 4 Mpc (Freeman et al. 1977), offers us an opportunity to study an active galactic nucleus (AGN) at high spatial resolutions ($1'' \sim 20$ pc). Located in a relatively unobscured region of the Galactic plane ($A_V \sim 1.5$ mag), Circinus is at an inclination of $\sim 65^\circ$, displays typical Seyfert 2 characteristics such as coronal lines (Oliva et al. 1994), a prominent Fe K α X-ray emission line (Matt et al. 1996), water vapor megamaser emission (Greenhill et al. 2003), and a prominent cone-shaped region of [O III] line emission (Wilson et al. 2000). The extended [O III] ionization cone was also observed by Veilleux & Bland-Hawthorn (1997), revealing a complex filamentary structure and matter undergoing expulsion from the nucleus. Finally, Marconi et al. (1994) detected a ring of starburst emission $\sim 10''$ from the nucleus.

Mid-IR observations of AGNs can reveal the often dust-enshrouded central regions because of the reduced effects of extinction where $A_{10\mu\text{m}} \sim (0.05\text{--}0.1)A_V$, environment-dependent (Roche & Aitken 1985; Lutz et al. 1996). Moreover, the blackbody spectrum for dust temperatures typical of those around AGNs peaks in this wavelength range. Ten micron imaging of Circinus by Krabbe et al. (2001; resolution $\sim 1''.1$) clearly detected extended, starburst-associated mid-IR emission and extended emission around the nucleus. Higher spatial resolution images (Siebenmorgen et al. 2004) from the ESO 3.6 m telescope found half the 10 μm flux arises in an unresolved core, and the rest is distributed primarily in north-south structures on a scale of $1''$.

In order to explore the mid-IR morphology at high spatial resolution, we obtained images of Circinus from Gemini South (GS). In § 2, we detail the observations and data reduction technique, and in § 3 we describe the results and discuss their implications.

2. OBSERVATIONS AND DATA REDUCTION

Observations of Circinus were made on 2004 February 2 using the GS mid-IR instrument, the Thermal-Region Camera Spectrograph (T-ReCS; Telesco et al. 1998; see Table 1). T-ReCS uses a Raytheon 320 \times 240 pixel Si:As IBC array, providing a plate scale of $0''.089$ pixel $^{-1}$. The detector was used in correlated quadruple sampling (CQS) mode (Sako et al. 2003). Images were obtained in the 8.74 μm ($\Delta\lambda = 0.78$ μm , 50% cut-on/off) and 18.33 μm ($\Delta\lambda = 1.5$ μm , 50% cut-on/off) filters using the standard chop-nod technique to remove time-variable sky background, telescope thermal emission, and so-called 1/f detector noise. The chop throw was $15''$, and the telescope was nodded every 30 s. The chop throw was fixed at 90° (east-west), but the instrument rotation projected to the sky was changed between data sets to verify that chopping or instrumental effects (uncorrected by CQS) did not affect any observed structure.

Data were reduced using in-house-developed IDL routines. The difference for each chopped pair for each given nod set is calculated, and the nod sets are then differenced and combined until a single image is created. Chopped pairs obviously compromised by cirrus, high electronic noise, or other problems were excluded.

HD 108903 observations (γ Cru, 10.89 Jy at 8.8 μm and 296.69 Jy at 18 μm) were made for flux calibration through both filters; 18.33 μm observations of γ Cru taken more than 2 hr apart showed a variation in counts less than 13%, typical of mid-IR photometry. While no flux standards were observed more than once at 8.74 μm , variations in that band are typically much less than at 18.33 μm . Point-spread function (PSF) observations, through both filters, were made immediately prior to or after the Circinus observations and used an identical setup to accurately sample the image quality. The 18.33 μm PSF was at an insufficient signal-to-noise ratio (S/N), and instead the flux calibrator was used as the PSF. The 8.74 μm FWHM was $0''.33$ (standard deviation $1\sigma \sim 0''.018$) and $0''.55$ in the 18.33 μm filter. Short PSF or flux standard observations are comparable to longer source observations, as the closed-loop active optics of GS provides a similar PSF when taken at a similar telescope pointing and time. Observations of PSF and flux standards through the night showed a stable PSF, and Circinus data sets showed no significant variations when divided into time increments equal to the PSF observations (~ 60 s at 8.74 μm). By rotating the

¹ Department of Astronomy, University of Florida, 211 Bryant Space Science Center, P.O. Box 112055, Gainesville, FL 32611-2055.

² Department of Astrophysics, Oxford University, Denys Wilkinson Building, Keble Road, Oxford OX1 3RH, UK.

³ Science and Technology Research Centre, University of Hertfordshire, Hatfield, Hertfordshire AL10 9AB, UK.

⁴ Joint Center for Astrophysics, Department of Physics, University of Maryland, Baltimore County, 1000 Hilltop Circle, Baltimore, MD 21250.

⁵ Departamento de Astrofísica Molecular y Infrarroja, Instituto de Estructura de la Materia (CSIC), Serrano 113b, 28006 Madrid, Spain.

TABLE 1
OBSERVING LOG FOR CIRCINUS AND PSF CALIBRATION

Filter (μm)	T-ReCS P.A. (deg)	Chop Frequency (Hz)	Circinus On-Source Time (s)	Average Air Mass
8.74	0	2.07	450	1.29
8.74	20	2.07	109	1.25
18.33	20	2.76	109	1.25

NOTE.—Units are as noted, and the T-ReCS P.A. is measured as the degree rotation east of north.

instrument to different position angles (P.A.'s), the data were confirmed to be consistent at different chop P.A.'s.

T-ReCS was mounted to the GS Cassegrain port so that north was up and east was left as projected to the detector. In post-processing, images of the PSF stars were derotated by $35^\circ 9$ (PPM 359894) and $95^\circ 6$ (HD 108903) at 8.74 and 18.33 μm , respectively, to match the telescope pupil P.A. when Circinus was observed. Image rotation is necessary because the projected angles of the telescope pupil (particularly the secondary mirror supports) rotate during observations (or pointings), having a significant effect on the low-level profile.

3. RESULTS

Figure 1 shows the contour images of the 8.74 μm band Circinus data and the PSF that most closely matches the air mass of the Circinus observations. Following Radomski et al. (2002) and Soifer et al. (2003), we employ various levels of scaled PSF subtraction to investigate the low-brightness regions around the central pointlike source. Figure 2 shows the 18.33 μm band data in a similar way. At both wavelengths, prominent extensions with a knotty morphology extend $\sim 2''$ east and west (P.A. $\sim 81^\circ$ and $\sim 278^\circ$, respectively) of the nucleus. The extent, P.A., and brightness distribution of both mid-IR extensions are coincident with the [Si vi] 1.96 μm (P.A. $\sim 80^\circ$ and $\sim 280^\circ$; Maiolino et al. 2000) emission-line distribution, clearly shown in Figure 3. The western mid-IR extension is coincident with the southern edge (P.A. $\sim 89^\circ$) of the compact (30 pc) V-shaped [O iii] $\lambda 5007$ (Wilson et al. 2000) emission-line cone (Fig. 3), as well as extended X-ray emission (Sambruna et al. 2001), if we assume a common peak emission. The [O iii] and [Si vi]

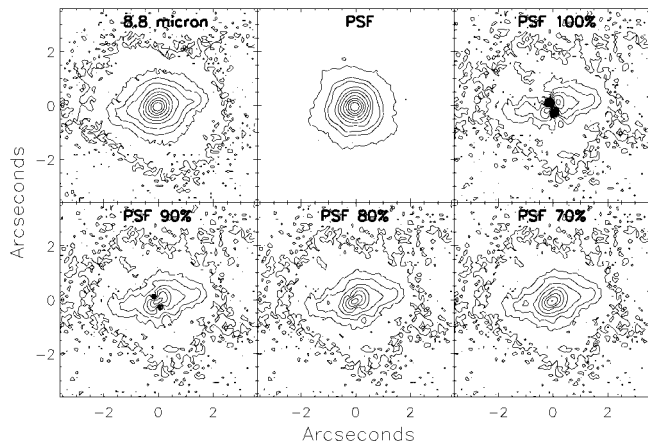


FIG. 1.—The 8.74 μm (8.8 μm) contour plots of Circinus, the PSF, and scaled subtraction of the PSF from Circinus. Contours are in a log scale, the lowest contour representing a 3σ detection at 0.27 mJy, followed by 0.93, 1.73, 3.23, 6.02, 11.23, 20.94, 39.07, 72.87, 135.93, and 253.55 mJy. Black areas near the nucleus represent regions of negative flux, an artifact from PSF subtraction.

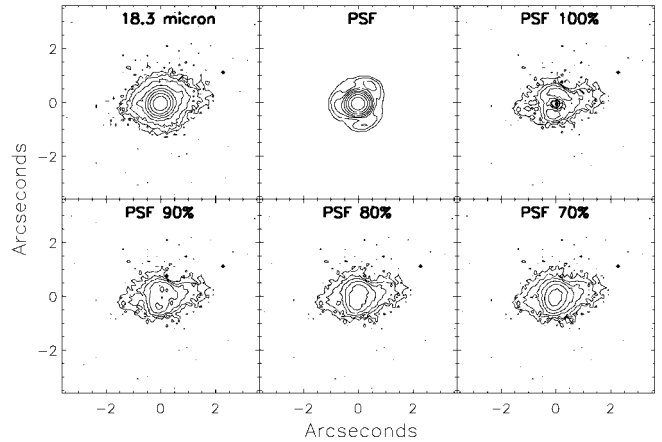


FIG. 2.—The 18.33 μm (18.3 μm) contour plots of Circinus, the PSF, and scaled subtraction of the PSF from Circinus. Contours are in a log scale, the lowest contour representing a 3σ detection at 4.716 mJy, followed by 7.86, 13.11, 21.85, 36.43, 60.74, 101.27, 168.83, and 281.46 mJy.

emission was interpreted as projections of sections of the ionization cones, where the brightest sections of the cone delineate areas of enhanced gas density (Maiolino et al. 2000).

N-band observations by Krabbe et al. (2001) from the ESO 2.2 m telescope detected diffuse emission $\sim 12''$ northeast from the nucleus and a tentative discovery of nuclear extended emission. Our data confirm their findings and, in the nuclear regions, provide detailed morphological and flux information absent in their data. Galactic emission is detected (not shown), but the limited GS chop throw ($15''$) partially overlapped the chopped beams, and hence both morphology and flux measurements of the galactic emission are compromised. Table 2 shows the flux

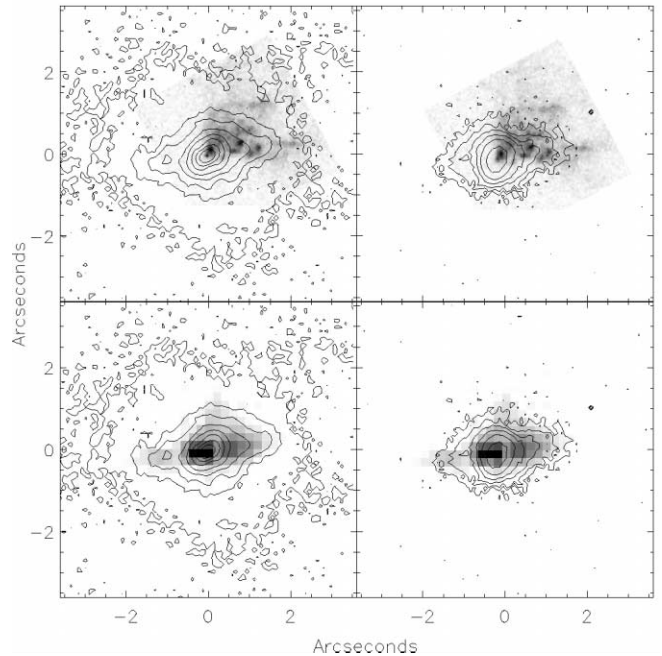


FIG. 3.—Upper panels: The 8.74 μm (left) and 18.33 μm (right) T-ReCS data (contour) overlaid onto the [O iii] emission-line map (gray scale) of Wilson et al. (2000). Lower panels: The 8.74 μm (left) and 18.33 μm (right) T-ReCS data (contour) overlaid onto the [Si vi] emission-line map (gray scale) of Maiolino et al. (2000). As no astrometry was available for the T-ReCS data, the peak emission of the T-ReCS data was matched to the central peak of the emission-line maps. T-ReCS contour maps show 70% PSF-scaled subtraction (see Fig. 1 and 2 legends for contour levels).

TABLE 2
PHOTOMETRIC DATA

Aperture	8.74 μm Flux (Jy)	18.33 μm Flux (Jy)
1"0 circle	5.51	12.90
3"5 circle	7.95	22.01
4"0 circle	8.16	22.81
5"0 circle	8.44	23.61
North	0.28	1.05
South	0.26	0.92
East	0.37	1.31
West	0.43	1.80

NOTES.—All flux densities are color-corrected and in units of janskys. The aperture sizes are as noted or are rectangular of size $1''.6 \times 0''.89$, centered $1''.42$ from the nucleus. While the 18.33 μm flux of the photometric standard varied by less than 13%, typical of mid-IR photometric accuracy, and the photometric variations in the 8.74 μm filter would have been significantly lower, these uncertainties dominate the photometric errors (see § 2).

measurements, where the uncertainty is dominated by photometric variations (§ 2). If the peak emission of the PSF is scaled to the peak of Circinus, the unresolved (PSF) component contributes $\sim 79\%$ of the total flux within a $5''$ aperture in the 8.74 μm wave band and $\sim 68\%$ in the 18.33 μm wave band. To estimate the emission from the extensions, we measured the flux contained within rectangles of size $1''.6 \times 0''.89$, centered $1''.42$ from the nucleus. Rectangular apertures were placed north, east, south, and west of the nucleus for both filters, and results are presented in Table 2.

3.1. Extended Emission

The western mid-IR extension is spatially coincident with enhanced [O III] and [Si VI] emission-line flux in the ionization cone. Based on integral field unit spectroscopic observations, Maiolino et al. (2000) suggest the enhanced emission-line flux arises as a result of gas streaming along the gaseous/dusty bar, supplying matter preferentially to one edge of the ionization cone. The material is ionized and ejected from the cone, detected by Veilleux & Bland-Hawthorn (1997) as far as 1 kpc from the nucleus. The spatial coincidence between the mid-IR emission and high-excitation emission lines suggests the same or related material is being detected in both cases at the ionization cone edge. Maiolino et al. (2000) suggest the gaseous/dusty bar likely extends through the nucleus and on both sides of the galactic disk; hence, the ionization cones interact with the bar on both sides. Viewed from our line of sight, one side of the gaseous/dusty bar was detected in near-IR color maps (Maiolino et al. 1998, 2000) as a linear-like feature, extending radially from the nucleus, shown schematically in Figure 4. Such a model readily accounts for the mid-IR extensions, with the eastern extension representing a direct detection of part of the “countercone.” This is consistent with the detection of the countercone in both near-IR polarized light (Ruiz et al. 2000) and the [Si VI] emission line (Maiolino et al. 1998, 2000). In order to investigate the specific mid-IR emission mechanism responsible for the extensions, we consider possible mechanisms below.

While no synchrotron emission has been observed in Circinus at optical or IR wavelengths, we investigate the possibility that a synchrotron jet, as detected in other AGNs (e.g., M87; Perlman et al. 2001), could be responsible for the extended mid-IR emission. At 8 GHz, the flux in the central $1''$ square region (Elmouttie et al. 1998) is ~ 100 mJy with a spectral index of $\alpha = -0.06$. One-zone synchrotron radiation models cannot produce a sudden upturn in the νF_ν spectrum, and hence a simple extrapolation of the radio synchrotron spectrum from

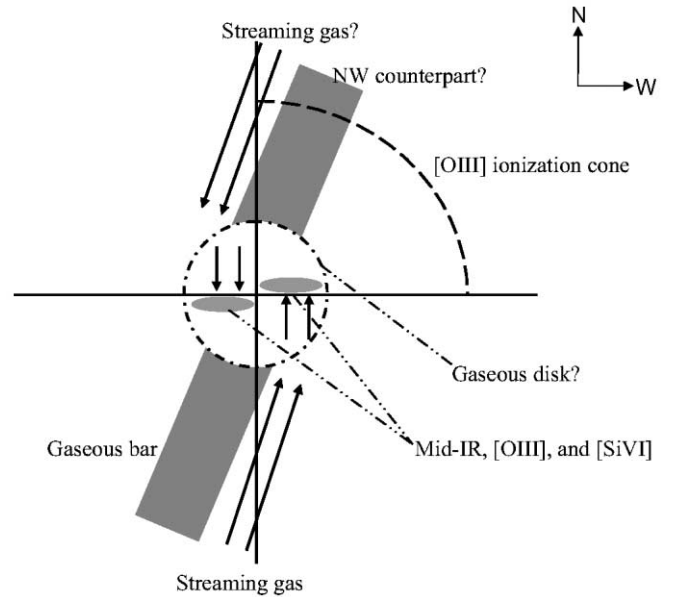


FIG. 4.—Schematic diagram of the central few 100 pc of Circinus, adapted from Fig. 2 of Maiolino et al. (2000). The center of the ionization cone is presumably the location of the AGN central engine. The northwest cone is pointing toward us, whereas the southeast cone points away, presumably obscured at optical wavelengths by the dusty disk of the host galaxy. The presence of a northwest gaseous bar and streaming gas were suggested from the Maiolino et al. (2000) observations but have not yet been observed.

the core flux underpredicts the 8.74 and 18.33 μm flux by more than a factor of 50.

Nuclear star formation regions were probed at high spatial resolution by Maiolino et al. (2000). Their $\text{Pa}\alpha$ 1.88 μm and [Fe II] 1.644 μm maps show significantly more diffuse emission than their [Si VI] map. Both the $\text{Pa}\alpha$ and [Fe II] emission-line maps are preferentially aligned along the major axis of the galaxy rather than the ionization cone, and therefore star formation cannot dominate emission in the extensions.

While prominent polycyclic aromatic hydrocarbon (PAH) emission was detected by the *Infrared Space Observatory* observations of the central $14'' \times 27''$ of the galaxy (Moorwood et al. 1996), ground-based spectroscopy at higher spatial resolution has isolated the nuclear emission and shows no evidence of PAH emission in the central few arcseconds, showing instead a deep silicate absorption band (Roche et al. 1991; Siebenmorgen et al. 2004). Therefore, the extensions cannot be dominated by PAH emission.

Mid-IR emission within ionization cones of AGNs due to dust heated by emission from the central engine has been observed in several other AGNs, such as NGC 1068 (Braatz et al. 1993) and Cygnus A (Radomski et al. 2002). In order to explore the plausibility of this mechanism in Circinus, we follow the methodology used for NGC 4151 by Radomski et al. (2003). The color ratio of the 8.74 and 18.33 μm bands yields a color temperature of $\sim 230 \pm 20$ K at a distance of $1''.5$ (30 pc) from the nucleus, if we assume optically thin emission. Dust grains in a strong UV field will primarily absorb that radiation and reemit in the IR, where the value of $Q_{\text{UV}}/Q_{\text{IR}}$ is dependent on the dust grain size and composition, given by Draine & Lee (1984), Laor & Draine (1993), and Weingartner & Draine (2001) for graphite and “smooth astronomical” (SA) silicate. The equilibrium temperature of the dust was determined by using the approach and, specifically, equation (1) from Radomski et al. (2003).

Given the nuclear luminosity of $\sim 2 \times 10^{10} L_\odot$ (Oliva et al.

1999) and equation (1) from Radomski et al. (2003) to estimate the dust grain size, the color temperature of the extensions is consistent with dust heated from a central ionizing source. Estimates for dust grain size, although small, are within limits of classical interstellar dust grains where the best-fitting dust size for (SA) silicate is ~ 0.003 or $\sim 0.015 \mu\text{m}$ for graphite grains with a range of ~ 0.003 – $10 \mu\text{m}$ (Laor & Draine 1993; Draine & Lee 1984).

These grain sizes are smaller than those estimated for centrally heated narrow-line region models of NGC 1068 ($\sim 0.05 \mu\text{m}$; Cameron et al. 1993), Cyg A ($\sim 0.1 \mu\text{m}$; Radomski et al. 2002), and NGC 4151 ($\sim 0.04 \mu\text{m}$ graphite or $0.01 \mu\text{m}$ SA silicate; Radomski et al. 2003). However, it has been argued that the hard photon flux from AGNs preferentially destroys small grains (Aitken & Roche 1985; Voit 1992) so that while direct heating by the central engine of Circinus can reproduce the observed grain temperatures, the small grain sizes required seem vulnerable in this environment. The spatial coincidence between the extended mid-IR emission and the near-IR high-excitation line emission suggests that nebular heating may be important. Maiolino et al. (2000) suggest that while a fraction of the near-IR emission lines could emanate from shock heating, a second mechanism must be at least partially responsible for the emission. Because of the close spatial correlation of the mid-IR to the near-IR [Si VI] line emission, the mid-IR emission probably (at least) partially arises through nonshock heating.

3.2. Unresolved Nuclear Emission

To investigate mid-IR emission associated with the presence of extended obscuring structures, we made nuclear photometric cuts, both perpendicular to the mid-IR extensions and the [O III] ionization cone axis. Photometric cuts at similar P.A.'s were also made for the PSF standard. The cuts were made only at $8.74 \mu\text{m}$, as this had the most complete set of PSF observations. The cuts at these P.A.'s show the central region PSF is indis-

tinguishable from the PSF standard. Following Soifer et al. (2000), we suggest extensions would be readily detected at 3 times the standard deviation of the PSF standard. For our data, $3\sigma = 0''.054 (\theta_{\text{sd}})$, based on three separate PSF observations. To find the maximum extension (θ_{max}), we use

$$\theta_{\text{max}}^2 = \theta_{\text{tot}}^2 - \theta_{\text{PSF}}^2, \quad (1)$$

where θ_{tot}^2 is $(\theta_{\text{PSF}} + \theta_{\text{sd}})^2$. Thus, any mid-IR extended emission at these P.A.'s must be $\leq 0''.20$ (diameter ≤ 4 pc) or have a flux density less than the 3σ S/N of the *N*-band data of 0.27 mJy.

The upper limit to the size of the nuclear mid-IR-emitting region is consistent with the upper limit for the torus outer radius (12 pc) inferred by (Ruiz et al. 2001) from modeling the nuclear spectral energy distribution (SED) of Circinus. The size of the unresolved mid-IR emitting region of Circinus is smaller than NGC 4151 (Radomski et al. 2003; Ruiz et al. 2003), consistent with the higher AGN luminosity of the latter galaxy. However, this size is similar to the SED-based estimate for Cen A (Alexander et al. 1999), despite Cen A's black hole having a mass ~ 100 times larger.

The outer radius at which molecular megamaser emission is detected in Circinus (Greenhill et al. 2003) is similar to the size limit of any mid-IR obscuring structure. Hence, we cannot exclude the possibility that the obscuring/collimating structure is a thin, warped disk of material associated with the maser emission.

We thank the referee for suggesting several improvements. C. P. and J. T. R. acknowledge NSF grant 0206617. E. P. acknowledges NASA grant NAG5-9997 (LTSA). Observations were obtained at the Gemini Observatory, operated by AURA, Inc., under agreement with the NSF on behalf of the Gemini partnership: NSF (US), PPARC (UK), NRC (Canada), CONICYT (Chile), ARC (Australia), CNPq (Brazil), and CONICET (Argentina).

REFERENCES

- Aitken, D. K., & Roche, P. F. 1985, *MNRAS*, 213, 777
 Alexander, D. M., Efstathiou, A., Hough, J. H., Aitken, D. K., Lutz, D., Roche, P. F., & Sturm, E. 1999, *MNRAS*, 310, 78
 Braatz, J. A., Wilson, A. S., Gezari, D. Y., Varosi, F., & Beichman, C. A. 1993, *ApJ*, 409, L5
 Cameron, M., et al. 1993, *ApJ*, 419, 136
 Draine, B. T., & Lee, H. M. 1984, *ApJ*, 285, 89
 Elmouttie, M., Haynes, R. F., Jones, K. L., Sadler, E. M., & Ehle, M. 1998, *MNRAS*, 297, 1202
 Freeman, K. C., Karlsson, B., Lynga, G., Burrell, J. F., van Woerden, H., Goss, W. M., & Mebold, U. 1977, *A&A*, 55, 445
 Greenhill, L. J., et al. 2003, *ApJ*, 590, 162
 Krabbe, A., Böker, T., & Maiolino, R. 2001, *ApJ*, 557, 626
 Laor, A., & Draine, B. T. 1993, *ApJ*, 402, 441
 Lutz, D., et al. 1996, *A&A*, 315, L269
 Maiolino, R., Alonso-Herrero, A., Anders, S., Quillen, A., Rieke, M. J., Rieke, G. H., & Tacconi-Garman, L. E. 2000, *ApJ*, 531, 219
 Maiolino, R., Krabbe, A., Thatte, N., & Genzel, R. 1998, *ApJ*, 493, 650
 Marconi, A., Moorwood, A. F. M., Origlia, L., & Oliva, E. 1994, *Messenger*, 78, 20
 Matt, G., Brandt, W. N., & Fabian, A. C. 1996, *MNRAS*, 280, 823
 Moorwood, A. F. M., et al. 1996, *A&A*, 315, L109
 Oliva, E., Marconi, A., & Moorwood, A. F. M. 1999, *A&A*, 342, 87
 Oliva, E., Salvati, M., Moorwood, A. F. M., & Marconi, A. 1994, *A&A*, 288, 457
 Perlman, E. S., Sparks, W. B., Radomski, J., Packham, C., Fisher, R. S., Piña, R., & Biretta, J. A. 2001, *ApJ*, 561, L51
 Radomski, J. T., Piña, R. K., Packham, C., Telesco, C. M., De Buizer, J. M., Fisher, R. S., & Robinson, A. 2003, *ApJ*, 587, 117
 Radomski, J. T., Piña, R. K., Packham, C., Telesco, C. M., & Tadhunter, C. N. 2002, *ApJ*, 566, 675
 Roche, P. F., & Aitken, D. K. 1985, *MNRAS*, 215, 425
 Roche, P. F., Aitken, D. K., Smith, C. H., & Ward, M. J. 1991, *MNRAS*, 248, 606
 Ruiz, M., Alexander, D. M., Young, S., Hough, J., Lumsden, S. L., & Heisler, C. A. 2000, *MNRAS*, 316, 49
 Ruiz, M., Efstathiou, A., Alexander, D. M., & Hough, J. 2001, *MNRAS*, 325, 995
 Ruiz, M., Young, S., Packham, C., Alexander, D. M., & Hough, J. H. 2003, *MNRAS*, 340, 733
 Sako, S., et al. 2003, *PASP*, 115, 1407
 Sambruna, R. M., et al. 2001, *ApJ*, 546, L9
 Siebenmorgen, R., Krügel, E., & Spoon, H. W. W. 2004, *A&A*, 414, 123
 Soifer, B. T., Bock, J. J., Marsh, K., Neugebauer, G., Matthews, K., Egami, E., & Armus, L. 2003, *AJ*, 126, 143
 Soifer, B. T., et al. 2000, *AJ*, 119, 509
 Telesco, C. M., Pina, R. K., Hanna, K. T., Julian, J. A., Hon, D. B., & Kisko, T. M. 1998, *Proc. SPIE*, 3354, 534
 Veilleux, S., & Bland-Hawthorn, J. 1997, *ApJ*, 479, L105
 Voit, G. M. 1992, *MNRAS*, 258, 841
 Weingartner, J. C., & Draine, B. T. 2001, *ApJ*, 548, 296
 Wilson, A. S., Shopbell, P. L., Simpson, C., Storchi-Bergmann, T., Barbosa, F. K. B., & Ward, M. J. 2000, *AJ*, 120, 1325